Modeling And Testing The Thermal Effect Of Lubricating Oil Sprayed In Sliding-Vane Air Compressors Using Pressure-Swirl Nozzles

Gianluca VALENTI[1,3]*, Stefano MURGIA[2], Ida COSTANZO[2],
Giulio CONTALDI[2], Alessandro VALENTI[3]

[1]Politecnico di Milano, Dip. Energia,
Milano, Italy
Contact Information (+39-02.2399.3845, gianluca.valenti@polimi.it)

[2]Ing. Enea Mattei S.p.a.,
Vimodrone (Milano), Italy
Contact Information (+39-02.2530.5283, stefano_murgia@mattei.it)

[3]Valenti Energie S.r.l.,
Segrate (Milano), Italy

* Corresponding Author

ABSTRACT

A number of studies report the benefit of proper oil spraying in positive-displacement compressors. This work presents a thermodynamic model for simulating sliding-vane air compressors that employ an injection system for the lubricating oil based on both plain orifices and pressure-swirl nozzles to exploit the thermal effect of sprayed oil inside the compression chambers. An experimental campaign on a large-size compressor is conducted measuring, among all, the pressure within a chamber. This measurement is used to validate the model. Oil droplet diameters depend strongly on the injection technology, nozzles generating a finer atomization than orifices, as well as the differential pressure. In any case, the proper positioning of the nozzles allows for an effective heat transfer from the air to the oil.

1. INTRODUCTION

Positive-displacement compressors and, among them, sliding-vane machines are widely used in the compressed air industry. As in other fields, the efficient utilization of energy is a major goal. Hence, the aim of this work is the numerical modeling and the experimental testing of the thermal effect due to spraying the lubricating oil inside sliding-vane air compressors using pressure-swirl nozzles. This effect can be exploited to reduce the compression work.

The benefit of proper oil spraying in positive-displacement compressors has been reported by a number of studies, starting from Singh and Bowman (1986) and from Stosic *et al.* (1988 and 1992) who investigated numerically and experimentally the potential advantage in screw compressors. Shortly later, Fujiwara and Osada (1995) confirmed those positive result still on screw machines. Recently, Valenti *et al.* (2013 and 2014) and Bianchi *et al.* (2014) have focused on sliding-vane compressors, highlighting the higher potential in this kind of machines thanks to their cylindrical shape that allows for a very effective oil spraying parallel to the axis of the compressor itself.

The novelty of this work resides in the extension of the previous model to describe more accurately the quantity and the diameter distribution of the oil droplets and, consequently, to predict more precisely the heat transfer between the oil and the air within a compression chamber. Importantly, *this extension allows not using any tuned parameter*. The model is implemented in a MATLAB code and employed to simulate an existing large-size sliding-vane air compressor that is equipped with both plain orifices and pressure-swirl nozzles. Simultaneously, an experimental campaign is conducted on that compressor measuring the pressure within the chambers by piezoelectric transducers and to reconstruct the pressure-angle diagram. The pressure measurement is used to validate the numerical results.

2. THERMODYNAMIC MODEL

A *pressure-swirl nozzle* is an atomizer that generates liquid droplets imparting a swirl motion to the fluid prior to entering an orifice. The centrifugal forces break the liquid as soon as it leaves the orifice, producing droplets of different dimensions (Lefebvre, 1989). To model this phenomenon, during compression process, a thermodynamic model is developed here as an extension of a previous work (Valenti *et al*., 2013). The extended model takes into account the *number* and the *position* of the injectors as well as their *jet characteristics*. The number influences the quantity of injected oil and the position influences the jet properties, while both influence the compression process.

When an *oil jet* enters a compression chamber, the related injector is said *activated* for that chamber. Moreover, the jet splits into a number of droplets of different dimensions. The fraction of the jet that breaks up into droplets of the similar size is named *class*. At the end of the compression process, all droplet classes of all injectors are present inside the chamber, assuming that the droplets do not collide against each other or against the chamber walls.

2.1 Process mathematical model

The analysis of the heat transfer between gas and liquid during the compression process is based on the following assumptions, which are the same as those employed in the previous work (Valenti *et al*., 2013):

- the gas behaves as an ideal gas and the liquid as an incompressible fluid, both having a constant specific heat;
- the gas is non-soluble into the liquid and the liquid non-volatile into the gas;
- the compression is adiabatic toward the surroundings;
- the droplets are non-deformable spheres and the coalescence of droplets is neglected;
- the temperature variation inside the droplets is neglected.

Regarding the last assumption on the temperature within a droplet, its variation can be practically neglected, as explained by Incropera and DeWitt (1996), if the following condition on the *Biot number* Bi [-] is satisfied:

$$Bi = \frac{h\,d}{6\,k_l} \leq 0.1 \tag{1}$$

where h is the convective heat transfer coefficient at the droplet surface [W m^{-2} K^{-1}], d is the droplet diameter [m], k_l is the liquid thermal conductivity [W m^{-1} K^{-1}]. In its turns, h can be evaluated from the *Nusselt number* Nu_d [-]:

$$Nu_d = \frac{h\,d}{k_g} \tag{2}$$

where k_g is the gas thermal conductivity [W m^{-1} K^{-1}]. In this study, Nu_d is always taken equal to 2 because this value corresponds, from the point of view of heat transfer, to the case of *pure conduction*, which is a conservative approach.

The *instantaneous energy balance* applied to a *single compression chamber* is:

$$\frac{dU_g}{dt} + \sum_{i=1}^{K} \frac{dU_{l,i}}{dt} = \dot{L} - \dot{Q}_{amb} \tag{3}$$

where U_g is the gas while U_l the liquid internal energy [J] and $\dot{L}$ the chamber compression power [W], taken positive if transferred to the chamber itself. $\dot{Q}_{amb}$ is the thermal power exchanged with the surroundings [W], neglected as a first approach so that the compression is considered adiabatic. K is the number of all liquid droplet classes present inside the chamber at any time step, reaching the maximum value at the end of the process when all injectors are activated. Furthermore, the instantaneous energy balance applied to the *liquid phase* is:

$$\frac{dU_{l,i}}{dt} = m_{l,i} c_l \frac{dT_{l,i}}{dt} = -h_i A_i \left(T_{l,i} - T_g\right) \qquad \forall i \in [1, K] \tag{4}$$

where i identifies each droplet class, while the instantaneous energy balance applied to the *gas phase* is:

$$\frac{dU_g}{dt} = m_g c_{v,g} \frac{dT_g}{dt} \tag{5}$$

In equations (4) and (5) m is the mass [kg], T the temperature [K], A the class heat transfer surface [m^2], given by the product of the number N of droplets and the surface of a single droplet for each class, c_l the liquid while $c_{v,g}$ the gas isochoric specific heat [J K^{-1} kg^{-1}].

The *chamber compression power* is equal to the gas compression power as the liquid is assumed incompressible. Thus:

$$\dot{L} = -p_g \frac{dV_g}{dt} \tag{6}$$

where p_g is the gas pressure [Pa] and V_g the gas volume [m^3]. In its turn, V_g is computed as:

$$V_g(t) = V(t) - V_l(t) \tag{7}$$

where V is the chamber volume [m^3] and V_l the liquid volume [m^3]. The chamber volume V is known, as it is calculated by geometrical means as a function of the angular position. Here, the angular position of a chamber is defined by the position of its trailing vane and starting from the tangent point between rotor and stator.

Finally, the *chamber pressure* is related to the volume and the temperature of the gas by the ideal gas equation of state:

$$p_g V_g = m_g R_g T_g \tag{8}$$

2.2 Process numerical model

The system of equations presented above is implemented using a *backward Euler method*. Rearranging the equations:

$$\begin{cases} m_g c_{v,g} {T_g}^{n+1} + \sum_{i=1}^{K} m_{l,i} c_l {T_{l,i}}^{n+1} = m_g c_{v,g} {T_g}^{n} + \sum_{i=1}^{K} m_{l,i} c_l {T_{l,i}}^{n} - p_g({V_g}^{n+1} - {V_g}^{n}) & (9) \\ -h_1 A_1 dt {T_g}^{n+1} + (m_{l,1} c_l + h_1 A_1 dt) {T_{l,1}}^{n+1} = m_{l,1} c_l {T_{l,1}}^{n} & (10) \\ \vdots \\ -h_K A_K dt {T_g}^{n+1} + (m_{l,K} c_l + h_K A_K dt) {T_{l,K}}^{n+1} = m_{l,K} c_l {T_{l,K}}^{n} & (11) \\ {p_g}^{n+1} = \frac{m_g R_g {T_g}^{n+1}}{{V_g}^{n+1}} & (12) \end{cases}$$

Equations (9) to (11) can be seen as a *linear system of equations*, with unknowns ${T_g}^{n+1}$and ${T_{l,i}}^{n+1}$. In matrix form:

$$\underline{\underline{A}}\,\underline{T} = \underline{b} \tag{13}$$

where $\underline{\underline{A}}$, $\underline{T}$ and $\underline{b}$ change size every time an injector is activated. As seen, when all injector are activated, K is equal to the total number of droplet classes (sum of all classes of all injectors) and the linear system reaches the maximum dimension. In particular, $\underline{\underline{A}}$ dimension is [1+ K; 1+ K] while $\underline{T}$ and $\underline{b}$ dimension is [K;1]. Mathematically:

$$\underline{\underline{A}} = \begin{bmatrix} m_g c_{v,g} & m_{l,1} c_l & m_{l,2} c_l & \cdots & m_{l,K} c_l \\ -h_1 A_1 dt & m_{l,1} c_l + h_1 A_1 dt & 0 & 0 & 0 \\ -h_2 A_2 dt & 0 & m_{l,2} c_l + h_2 A_2 dt & 0 & 0 \\ \vdots & 0 & 0 & \ddots & 0 \\ -h_K A_K dt & 0 & 0 & 0 & m_{l,K} c_l + h_K A_K dt \end{bmatrix} \tag{14}$$

as well as:

$$\underline{T} = \begin{bmatrix} {T_g}^{n+1} \\ {T_{l,1}}^{n+1} \\ \vdots \\ {T_{l,K}}^{n+1} \end{bmatrix} \tag{15}$$

and:

$$\underline{b} = \begin{bmatrix} m_g c_{v,g} {T_g}^{n} + \sum_{i=1}^{K} m_{l,i} c_l {T_{l,i}}^{n} - p_g({V_g}^{n+1} - {V_g}^{n}) \\ m_{l,1} c_l {T_{l,1}}^{n} \\ \vdots \\ m_{l,K} c_l {T_{l,K}}^{n} \end{bmatrix} \tag{16}$$

Solving numerically the system, gas and liquid temperatures at any time step n can be calculated. Ultimately, the gas pressure at each step is computed via Equation (12).

2.3 Pressure-swirl nozzle and plain orifice models

For *pressure-swirl nozzles*, the jet is described by the *Rosin-Rammler relation* as detailed by Mugele and Evans (1951):

$$f(d) = q\,\frac{d^{q-1}}{SMD^{q}}\,e^{-\left(\frac{d}{SMD}\right)^{q}} \tag{17}$$

where SMD is the *Sauter Mean Diameter*, defined as the diameter of a sphere that has the same volume-to-surface area ratio of the entire droplet sample, and q is the shape parameter providing a measure of the spread of droplet sizes. In its turn, q is taken equal to 3.5 (Lefebvre, 1989) and SMD computed via the relation by Wang and Lefebvre (1987):

$$SMD = 4.52\left(\frac{\sigma_l\,{\mu_l}^2}{\rho_g\,\Delta p^2}\right)^{0.25}\left[2.7\left(\frac{D_{or}\,\dot{m}_l\,\mu_l}{\rho_l\,\Delta p}\right)^{0.25} cos\frac{\gamma}{2}\right]^{0.25} + 0.39\left(\frac{\sigma_l\,\rho_l}{\rho_g\,\Delta p}\right)^{0.25}\left[2.7\left(\frac{D_{or}\dot{m}_l\,\mu_l}{\rho_l\,\Delta p}\right)^{0.25} cos\frac{\gamma}{2}\right]^{0.75} \tag{18}$$

where σ_l is the liquid surface tension [mN m^{-1}], Δp the differential pressure [Pa], ρ the density [kg m^{-3}], D_{or} the nozzle/orifice diameter [m], γ the cone spray angle [rad], $\dot{m}_l$ and μ_l are the liquid mas flow rate [kg s^{-1}] and viscosity [Pa s]. The droplet diameter depends strictly on the nozzle differential pressure, which is calculated as the difference between the injection pressure and the pressure inside the compression chamber at the moment of injection. The *injection pressure* is the same for all nozzles and equal to the compressor delivery pressure minus the pressure drop along the oil circuit. Figure 1 shows the effect of the differential pressure on SMD. The pressure depends strictly on the injector position: the closer the nozzle to the discharge port (i.e. Nozzle 4, as described in Section 3), the smaller the differential pressure and, thus, the bigger the droplet diameter. Lastly, the *mass flow rate through the nozzle* is derived, considering the liquid density, from a correlation provided by the manufacturer for the volume flow rate:

$$\dot{V}_l = F\,\dot{V}_2 = F\,\dot{V}_1\,\left(\frac{\Delta p_2}{\Delta p_1}\right)^{0.4} \tag{19}$$

where $\dot{V}_l$ is the volume flow rate [l min^{-1}] and Δp is the pressure difference across the nozzle [Pa]. Subscripts 1 and 2 identify two different test conditions: the first is associated to the manufacturer test condition with water while the second to the actual one with lubricant oil. F is a density conversion factor, in this case equal to 1.06.

For *simple plain orifices*, only one droplets class is considered because this kind of atomizers is not able to produce a fine atomized jet. The SMD of this class is evaluated via the correlation by Varde *et al*. (1984):

$$SMD = 8.7\,D_{or}\,(Re\,We)^{-0.28} \tag{20}$$

where Re [-] is the Reynolds and We [-] the Weber number. Lastly, the *mass flow rate through the orifice* is derived from Bernoulli equation taking a discharge coefficient C_d of 0.772, calculated according to Lichtarowicz *et al* (1965):

$$C_d = \frac{1}{\frac{1}{C_{du}} + 20\frac{(1 + 2.25\frac{L}{D_{or}})}{Re}} \tag{21}$$

where L [m] is the orifice length and C_{du} the ultimate discharge coefficient, defined as:

$$C_{du} = 0.827 - 0.0085\frac{L}{D_{or}} \tag{22}$$

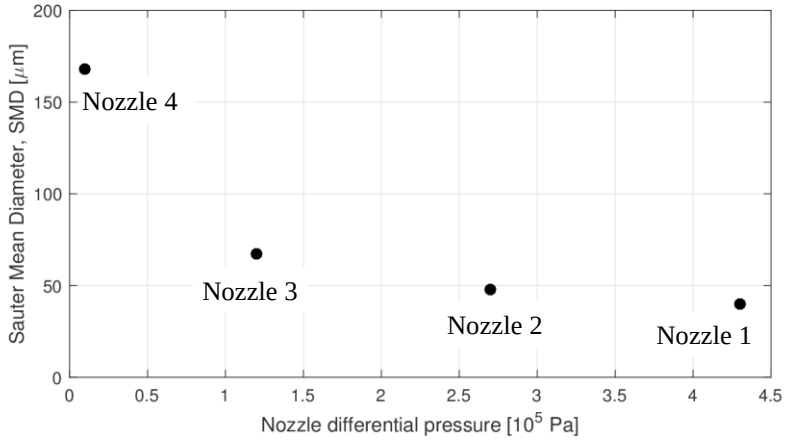

Figure 1: Effect of differential pressure on droplet SMD for each pressure-swirl nozzle of the considered compressor.

2.4 Lubricant oil property models

The thermo-physical properties of the liquid phase, which is the lubricating oil, are evaluated using semi-empirical correlations tuned with experimental data from the oil supplier. However, one parameter rarely available is the surface tension σ_l [mN m^{-1}], which is here calculated as (Brock and Bird, 1955):

$$\sigma = {p_c}^{2/3}\,{T_c}^{1/3} Q\,\left(1-\frac{T}{T_c}\right)^{11/9} \tag{23}$$

in which:

$$Q = 0.1196\left[1+\frac{\frac{T_b}{T_c}\ln\left(\frac{p_c}{1.01325}\right)}{1-\frac{T_b}{T_c}}\right]-0.2793 \tag{24}$$

where p_c [bar] and T_c [K] are respectively pressure and temperature at the critical point of the oil, and T_b [K] temperature at the normal boiling point (NBP). These can be evaluated according to the methodology proposed by Conde (1996), which makes use of two equations simultaneously. The first equation is that by Nokay (1959):

$$T_c = 15.2762\,S^{0.2985}{T_b}^{0.62164} \tag{25}$$

and the second that by Kesler and Lee (1976):

$$T_c = 189.8 + 450.6\,S + (0.4244 + 0.1174\,S)\,T_b + (0.1441 - 1.0069\,S)\,\frac{10^5}{T_b} \tag{26}$$

where S is the specific gravity, equal to the ratio between the liquid density and that of pure liquid water at 60°F (15.56°C). Solving these two equations simultaneously, T_b and T_c can be evaluated. Kesler and Lee (1976) proposed also the following equation for the critical pressure:

$$\begin{aligned}\ln p_C = {} & 17.2019 - 0.0566\,S^{-1} - (0.4364 + 4.1216\,S^{-1} + 0.21343\,S^{-2})\,10^{-3}\,T_b \\ & + (4.7579 + 11.819\,S^{-1} + 1.5302\,S^2)\,10^{-7}{T_b}^2 - (2.4505 + 9.9009\,S^{-2})10^{-10}{T_b}^3\end{aligned} \tag{27}$$

2.5 Diameter and probability of droplet classes

Each droplet class is characterized by a diameter and a probability. From the Rosin-Rammler droplet size distribution seen in Equation (17), the mean α and the variance β^2 of the function are calculated as (Montgomery *et al*., 2011):

$$\alpha = SMD\;\Gamma\left(1+\frac{1}{q}\right) \tag{28}$$

and:

$$\beta^2 = SMD^2\left\{\Gamma\left(1+\frac{2}{q}\right)-\left[\Gamma\left(1+\frac{1}{q}\right)\right]^2\right\} \tag{29}$$

where Γ is the Gamma function. For each nozzle, its droplet classes are identified by a vector $\underline{\varphi}$, determined from α and β: each element of the vector $\varphi(i)$ is a representative diameter for all droplets whose diameters fall in the interval $\varphi(i) \pm \beta/2$. In the case here adopted of five classes, the diameters of these classes are:

$$\underline{\varphi} = \{\alpha - 2\beta;\ \alpha - \beta;\ \alpha;\ \alpha + \beta;\ \alpha + 2\beta\} \tag{30}$$

The probability of a class of a nozzle $\varphi(i)$, that is the fraction of the mass flow rate though that nozzle breaking into droplets of diameters in that class interval, is determined exploiting the property of a probability density function:

$$\int_{-\infty}^{+\infty} f(x)\,dx = 1 \tag{31}$$

Geometrically, the probability of the class is the area of a rectangle centered in $\varphi(i)$ with base β. The heights of the second to the last intervals are calculated according to the *mean value theorem for integrals*, while the heights of first and last intervals, which are identical, are taken so that the sum of all rectangle areas is unity.

3. EXPERIMENTAL TEST

Simultaneously to the development of the thermodynamic model, an experimental campaign is conducted on a *large-size sliding-vane air compressor* that adopts *two oil injection systems* in order to validate the model:

- plain orifices on the lateral surface of the stator along the axis and positioned close to the discharge port;
- four couples of pressure-swirl nozzles on both end plates distributed from the suction to the discharge port.

The *test rig* for the experimental campaign comprises an absolute pressure transducer to measure pressure of the ambient air and a group of T-type thermocouples placed on the compressor stator near the inlet valve to measure the initial compression temperature (Figure 2). An additional T-type thermocouple indicates the injected oil temperature. Four piezoelectric transducers, placed circumferentially along one end plate, measure the pressure along the process (Figure 3). The measurement uncertainties of the adopted sensors are listed in Table 1. Ultimately, the pressure data acquired from the piezoelectric transducers are post-processed to reconstruct *the pressure-angle diagram* following the methodology defined by Cipollone et al. (2009).

The *test case* is characterized by ambient pressure of 100325 Pa and injected oil temperature of 60°C. The compressor delivery pressure is 7.5 bar(g) and the angular speed is 990 rpm.

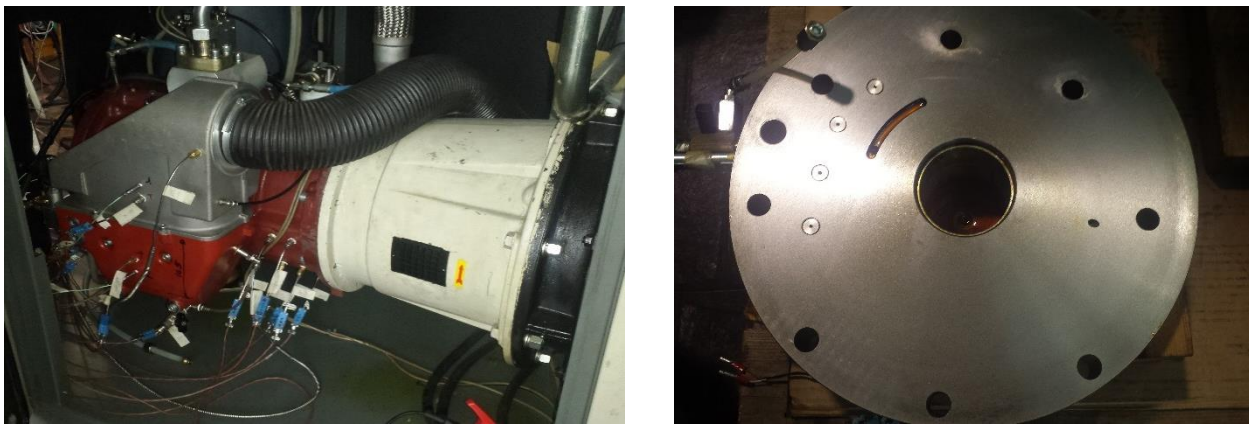

Figure 2: The considered large-size sliding-vane air compressor. Left: group of T-type thermocouples (see blue connectors) placed on the stator near the inlet valve. Right: four pressure-swirl nozzles placed on one end plate.

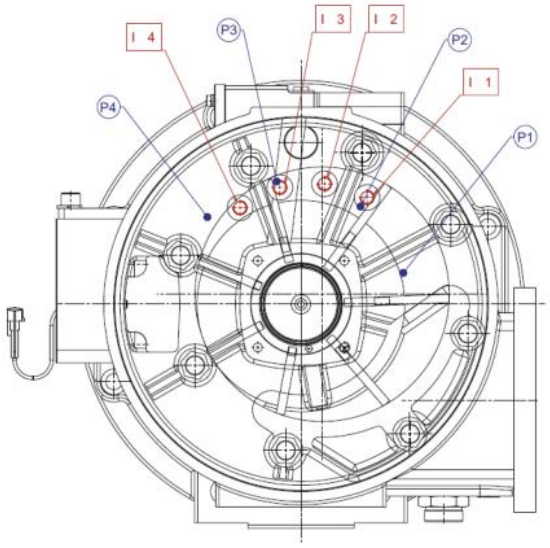

Figure 3: Position of the pressure-swirl nozzles and of the piezoelectric pressure transducers on one end plate. "I" indicates nozzles while "P" transducers.

Table 1: Measurement sensors and uncertainties.

Instrument type	Quantity, unit	Absolute uncertainty
T-type thermocouple	Temperature, °C	0.5
Absolute pressure transducer	Pressure, bar	0.08
Piezoelectric pressure transducer	Pressure, bar	0.01

4. RESULTS AND VALIDATION

The geometrical features of the considered compressor are utilized to determine the chamber volume V as a function of the angular position. Next, the process in the compressor is simulated with the thermodynamic model described in Section 2 and the thermo-physical properties for air and lubricant oil listed in Table 2. In particular, each of the four pressure-swirl nozzle jets is described dividing the droplets into five classes, as presented in Section 2.4, to take into account their fine nebulization, whereas plain orifice jets only in a single class, yielding 21 total classes.

The resulting class diameters for each pressure-swirl nozzle jet are shown in Figure 4. Nozzle 1, which is the closest to the suction port exploiting the highest differential pressure Δp, is characterized by very fine dimensions, from 13 µm to 59 µm. Nozzle 5, instead, from 55 µm to 247 µm. In contrast, the plain orifices are characterized by a class of 800 µm. Figure 5 shows the temperature of all classes during the compression process. Temperature of bigger droplets (Class 5) increases by only a fraction of degree, but that of smaller ones (Class 1) increases even by over 50°C thanks to a very effective heat transfer from the air being compressed to the droplets, resulting in a non-adiabatic air compression. The calculated average oil temperature increase, which is the mass-averaged of all classes, is 12.1°C.

Additionally, Figure 6 shows the comparison between the measured and the calculated pressure within a compression chamber. The absolute value of the relative error is always below 5% and it is averagely equal to 2.3%. The relative error reaches higher values in the last part of the process, where the numerical model underestimates the real process. This is likely due to two effects. First, neglecting the coalescence of droplets and the collision on the chamber walls, the model assumes that all droplets are active until the end of the compression process, which is improbable. Second, the last part may be affected by leakages into the chamber from the discharge port, here not yet considered.

Table 2: Assumed parameters for the thermo-physical properties of the gas (air) and the liquid (lubricating oil).

Parameter	Symbol	Unit	Value
Gas (Air)			
Name			Air
Gas specific constant	R_g	J kg^{-1} K^{-1}	287.1
Isochoric specific heat	$c_{v,g}$	J kg^{-1} K^{-1}	720
Liquid (Lubricating oil)			
Name			Oil
Density	ρ_l	kg m^{-3}	930
Viscosity at 40°C	μ_l	Pa s	0.05
Isobaric specific heat	c_l	J kg^{-1} K^{-1}	1842
Compression			
Inlet gas temperature	$T_{g,0}$	K	338.15
Inlet liquid temperature	$T_{l,0}$	K	333.15

5. CONCLUSIONS

This work presents a thermodynamic model developed for positive-displacement compressors, in particular air sliding-vane machines, that employ a lubricant oil injection system based on plain orifices and/or pressure-swirl nozzles to exploit the thermal effect of spraying the oil inside the compression chambers. An experimental campaign is conducted measuring, among all, the pressure within a chamber, used for the validation. Conclusions are as follows.

- Diameters of droplet classes depend strongly on the injection technology and on the differential pressure, which depends on the position of the orifice or nozzle. Class diameters can be as small as 13 µm for the nozzle at the highest differential pressure, as large as 247 µm for that at the lowest, or 800 µm for the orifices.
- Heat transfer from the air to the lubricating oil droplets depends strongly on the droplet diameters. Temperature of the bigger droplets increase by a fraction of degree, but that of the smaller ones increases even by over 50°C. Average temperature increase is 12.1°C, resulting into a non-adiabatic air compression.
- The model is validated comparing the measured and the calculated pressure within a compression chamber. The relative error is within 5% and averagely equal to 2.3% despite the model does not use tuned parameters.

In short, *air is being cooled by the oil*. The *future work* will investigate further the phenomena that have a negative impact on the heat transfer, as the coalescence of droplets and their collision on the chamber walls, as well as leakages.

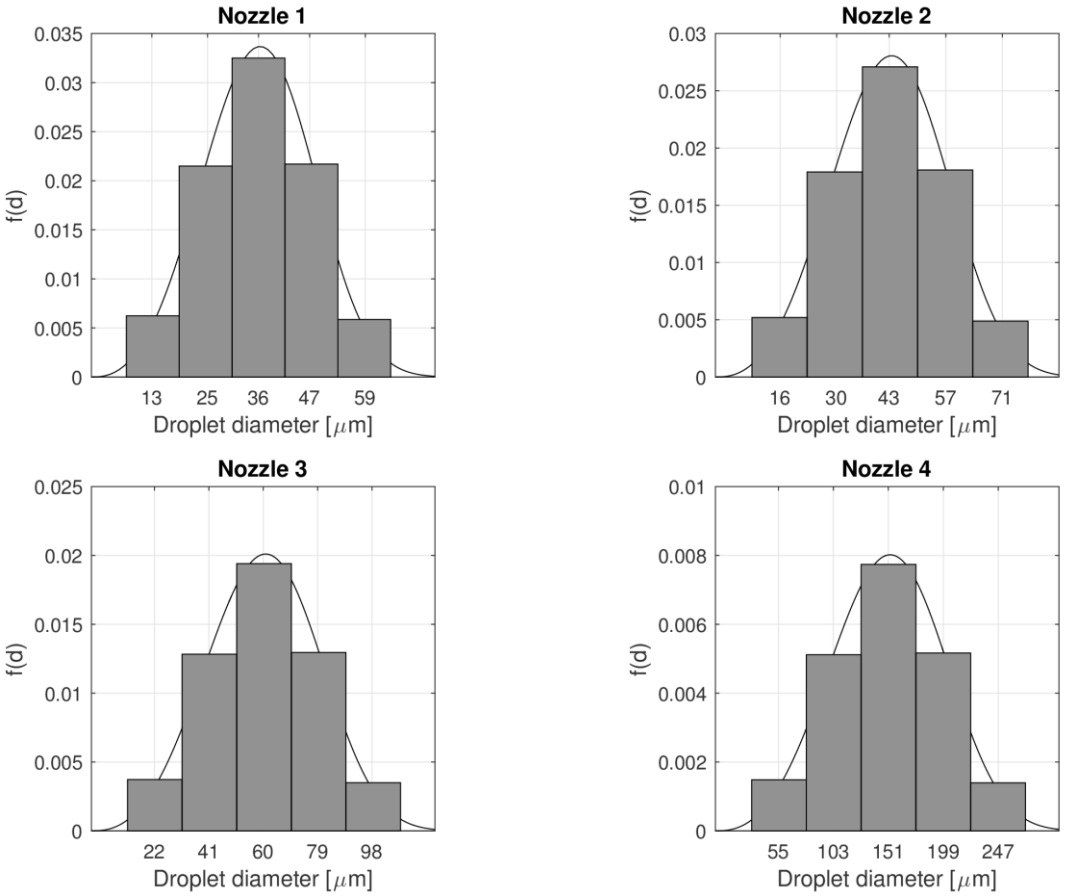

Figure 4: Rosin-Rammler probability density functions and calculated classes of the four pressure-swirl nozzles.

NOMENCLATURE

Symbols

Γ	Gamma function	(-)	Re	Reynolds number	(-)
Δ	difference	(-)	S	specific gravity	(-)
α	mean	(m)	SMD	Sauter Mean Diameter	(m)
β^2	variance	(m^2)	T	temperature	(K)
γ	cone spray angle	(rad)	$\underline{T}$	vector of temperatures	(K)
μ	viscosity	(Pa s)	U	internal energy	(J)
ρ	density	(kg m^{-3})	$\dot{V}$	volumetric flow rate	(l min^{-1})
σ	surface tension	(mN m^{-1})	V	volume	(m^3)
$\underline{\varphi}$	vector of droplet diameters	(m)	We	Weber number	(-)
A	heat transfer area	(m^2)	$\underline{b}$	vector	(J)
$\underline{\underline{A}}$	matrix of coefficient	(J K^{-1})	c	mass specific heat	(J kg^{-1} K^{-1})
Bi	Biot number	(-)	d	droplet diameter	(m)
C_d	discharge coefficient	(-)	h	heat transfer coefficient	(W m^{-2} K^{-1})
F	density correction factor	(-)	k	thermal conductivity	(W m^{-1} K^{-1})
K	droplets classes number	(-)	m	mass	(kg)
$\dot{L}$	compression power	(W)	n	time step	(-)
L	orifice length	(m)	p	pressure	(Pa)
N	number of droplets	(-)	q	size distribution parameter	(-)
Nu_d	Nusselt number	(-)	t	time	(s)
$\dot{Q}$	thermal power	(W)	x	generic variable	(-)
R	gas constant	(J kg^{-1} K^{-1})			

Subscript

amb	ambient	or	orifice
b	at normal boiling point	p	at constant pressure
c	at critical point	v	at constant volume
g	gas	i	droplets class identifier
l	liquid	0	inlet condition

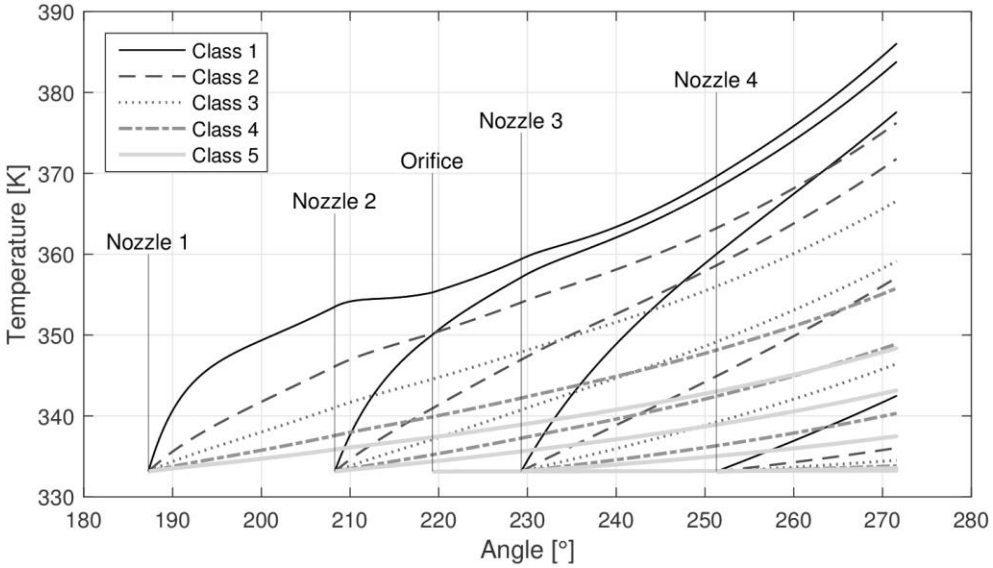

Figure 5: Calculated oil temperature as function of the angular position. Each injector is activated at a different angular position. In particular, it is possible to distinguish pressure-swirl nozzle jets, plain orifice jet, and the evolution of temperature of each class of droplets (Class 1 is the smallest for each nozzle, while Class 5 the biggest).

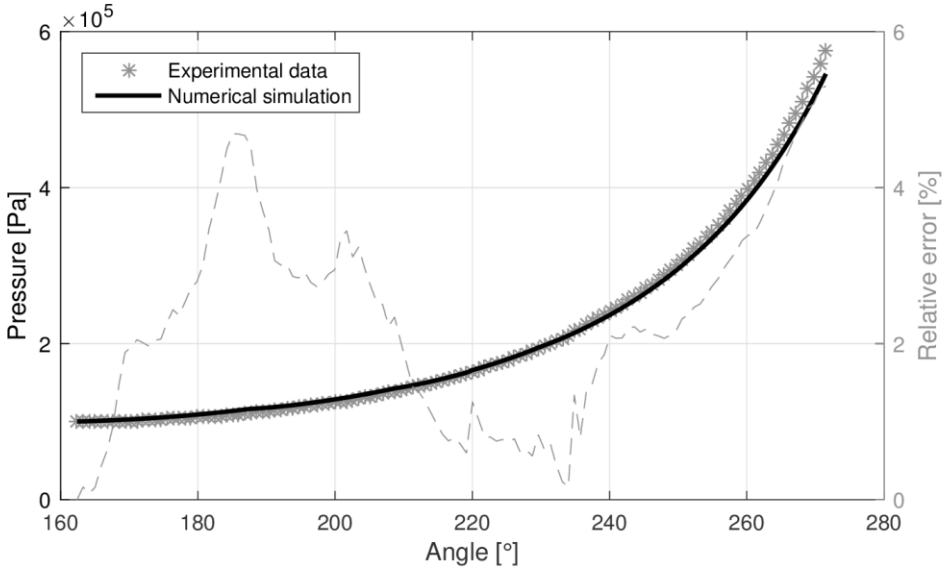

Figure 6: Numerical model validation. Comparison between the measured and the calculated pressure (left axis) and the absolute value of the relative percent error (right axis).

REFERENCES

Bianchi, G., Cipollone, R., Murgia, S., & Contaldi, G. (2014). Performance enhancement in sliding vane rotary compressors through a sprayed oil injection technology. In *Proceeding of the International Compressor Engineering Conference*. Paper Purdue, Lafayette, IN, USA.

Brock, J.R. & Bird, R. B. (1955). Surface tension and the principle of corresponding states. *AIChE Journal, 1*(2), 174-177. doi:10.1002/aic.690010208

Cipollone, R., Contaldi, G., Capoferri, A., & Valente, R. (2009). Theoretical and experimental study of the p-V diagram for a sliding vane rotary compressor, In *Proc. IMechE International Conference on Compressors and Their Systems (279-289)*, London, UK.

Conde, M. R. (1996). Estimation of thermo physical properties of lubricating oils and their solutions with refrigerants: An appraisal of existing methods. *Applied Thermal Engineering*, *16*(1), 51–61. doi:10.1016/1359-4311(95)00011-2

Fujiwara, M., & Osada, Y. (1995). Performance analysis of an oil-injected screw compressor and its application. *International Journal of Refrigeration*, *18*(4), 220-227. doi:10.1016/0140-7007(95)00008-Y

Incropera, F.P., & DeWitt, D.P. (1996). *Introduction to heat transfer.* New York, NY, USA: John Wiley & Sons.

Kesler, M.G., & Lee, B.I. (1976). Improved prediction of enthalpy of fractions. *Hydrocarbon Proc. 55*(3), 153-158.

Lefebvre, A.H. (1989). *Atomization and Sprays*. New York, NY, USA. Hemisphere Publishing Corporation.

Lichtarowicz, A.K., Duggins, R.H., & Markland, E. (1965). Discharge Coefficients for Incompressible Non-Cavitating Flow Through Long Orifices. *Journal of Mechanical Engineering Science. 7*(2), 210-219. doi:10.1243/JMES_JOUR_1965_007_029_02

Montgomery D.C., Runger G.C., & Hubele N.F. (2011). *Engineering statistics.* New York, USA: John Wiley & Sons.

Mugele, R.A., & Evans, H.D. (1951). Droplet Size Distribution in Sprays. *Ind. Eng. Chem., 43*(6), 1317–1324. doi:10.1021/ie50498a023

Nokay, R. (1959). Estimate petrolchemical properties. *Chem. Eng.*, *66*(2), 147-148.

Singh, P.J., & Bowman, J.L. (1986). Heat transfer in oil-flooded screw compressors. In *Proceedings of the International Compressor Engineering Conference (135-152).* Purdue, Lafayette, IN, USA.

Stosic, N., Kovacevic, A., Hanjalic, K., & Milutinovic, L. (1988). Mathematical modelling of the oil influence upon the working cycle of screw compressors. In *Proceeding of the International Compressor Engineering Conference (354-361)*. Purdue, Lafayette, IN, USA.

Stosic N., Milutinovic, L., Hanjalic, K., & Kovacevic, A. (1992). Investigation of the influence of oil injection upon the screw compressor working process. *Int. J. of Refrigeration, 15*(4), 206-220. doi:10.1016/0140-7007(92)90051-U

Valenti, G., Colombo, L., Murgia, S., Lucchini, A., Sampietro, A., Capoferri, A., & Araneo, L. (2013). Thermal effect of lubricating oil in positive-displacement air compressors. *Applied Thermal Engineering, 51*(1-2), 1055-1066. doi:10.1016/j.applthermaleng.2012.10.040

Valenti, G., Murgia, S., Contaldi, G., & Valenti, A. (2014). Experimental evidence of the thermal effect of lubricating oil sprayed in sliding-vane air compressors. *Case Studies in Thermal Engineering, 4*, 113-117. doi:10.1016/j.csite.2014.08.001

Varde, K., Popa, D., & Varde, L. (1984). Spray Angle and Atomization in Diesel Sprays, *SAE Technical Paper, 841055*. doi:10.4271/841055

Wang, X.F., & Lefebvre, A.H. (1987). Mean Drop Sizes from pressure-swirl nozzles. Journal of Propulsion and Power, 3(1), 11-18. doi:10.2514/3.22946